Investigation of the influence of the temporal convergence, spacial discretisation and geometry simplification for the numerical assessment of erosion-sensitive areas at an ultrasonic horn.

Stephan Mottyll[1], Saskia Müller[1], Jeanette Hussong[1], Romuald Skoda[1]

[1] *Ruhr-Universität Bochum, Chair of Hydraulic Fluid Machinery, 44801 Bochum, Germany, Email: stephan.mottyll@rub.de*

Introduction

In a numerical 3D study we simulate ultrasonic cavitation at an ultrasonic horn in order to investigate the cavitation erosion at the material surface. In contrast to other authors, e.g. Dular et al. [1] we apply a compressible CFD flow algorithm [2]. The main advantage of this method is the possibility to capture compressible wave dynamics, which are directly associated with the assessment of cavitation erosion [3]. The ultrasonic horn setup investigated consists of an oscillating horn tip (frequency $f = 20\,kHz$; amplitude $\hat{A}_{pp} = 40\,\mu m$), which is located $0.5\,mm$ above a counter sample. Both samples are circular with a diameter of $16\,mm$. To estimate the numerical error of our model for the temporal and spatial discretisation, we investigate the following numerical error sources: (1) spatial discretisation; (2) temporal convergence behaviour; (3) geometry simplifications.

Underlying numerical method

We use a compressible density-based flow algorithm with explicit time integration scheme (4th Order Runge-Kutta) and a fixed CFL-number (based on the speed of sound, $CFL < 1$). The convective fluxes are modelled with a Low-Mach-number consistent Gudonov-type flux formulation [2] which accounts for the pressure wave propagation in low-compressible liquids. We assume a homogeneous mixture of liquid and vapour, assuming both phases to be in thermodynamic equilibrium and phase change following an isentropic path [4]. Hence, the density is only dependent on pressure, which has been realised by a barotropic equation of state. To evaluate the erosion-sensitive areas we use a statistical analysis of transient wall loads in combination with predefined threshold values referred to as erosion probability P_{comb} for two combined erosion indicators: wall pressure and condensation rate. For a detailed description of the erosion analysis procedure refer to the previous publication [5].

Numerical error analysis

(1) Spatial discretisation: We perform a grid sensitivity study for a 90° segment geometry on three grids gradually refined by a factor of 1.2. For these grids we compare the erosion-sensitive areas for an analysis time interval from 2.8 to 10 ms.

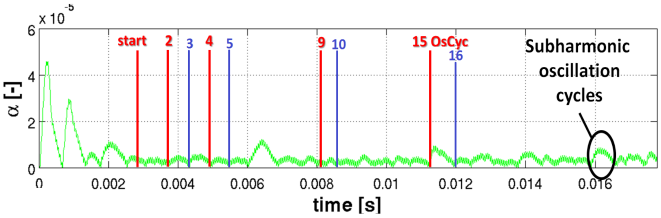

Figure 1: Integral vapour volume fraction α over time for different time intervalls from "start" point of erosion analysis till a fixed number of considered subharmonic oscillation cycles (360 driving cycles of the ultrasonic horn).

(2) Temporal convergence behaviour: We compare the predicted erosion-sensitive areas for different time intervals on a 90° segment geometry with coarsest grid resolution (horn tip sample). The expansion and collapse of vapour clouds occur on subharmonic time scales (related to the driving frequency of 20kHz, cf. Figure 1). Starting the erosion analysis at $t_{start} = 2.8ms$ we vary the number of these subharmonic oscillation cycles taken into account, in order to investigate the temporal convergence behaviour. As the convergence criterion we apply the average deviation of the ambit averaged erosion probability (f_{av}, cf. Figure 3) between a subsequently elongated time interval considerung n subharmonic oscillation cycles compared to a time interval considering one more subharmonic oscillation cycle ($n+1$, cf. Figure 1).

(3) Geometry simplification: We simulate the ultrasonic horn on a 360° geometry as well as on a 90° rotationally symmetric segment geometry on the coarsest grid for an analysis time interval from 2.8 to 10 ms and compare the predicted erosion-sensitive areas.

Results

The outcome of the three numerical error analyses can be concluded in the following results:

- After $n = 10$ subharmonic oscillation cycles an average error f_{av}<4% (quality criterion) is reached. This criterion can be reached independently of the grid resolution and the predefined erosion probability threshold.
- The distribution of erosion-sensitive areas (region with maximal erosion probability) can already be

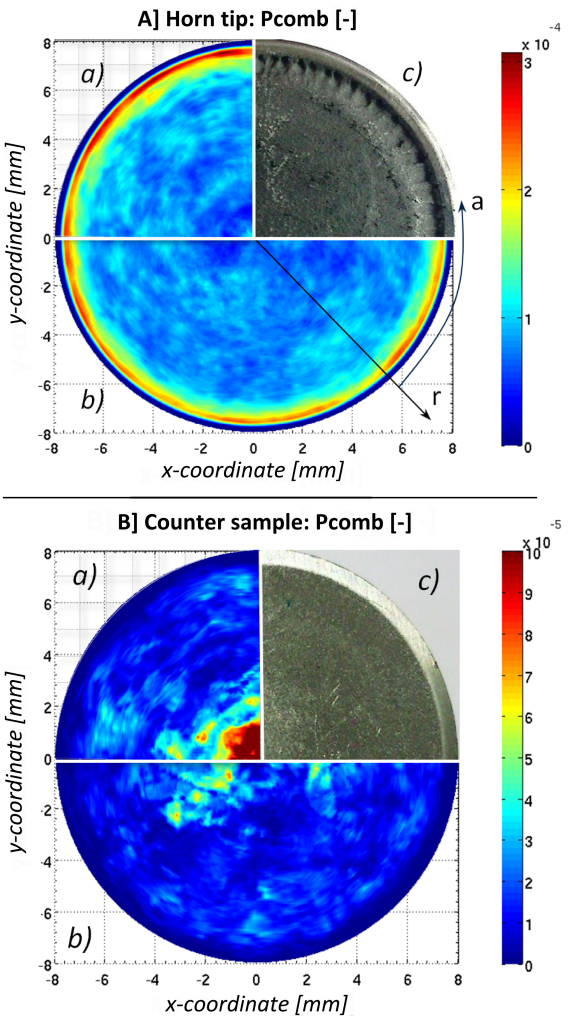

Figure 2: Erosion probability P_{comp} at A] the horn tip and B] the counter sample surface for a 90° segment geometry (a) as well as for a 360° complete geometry (b) compared with an image of erosion damage at the horn tip surface (c).

qualitatively captured after 2 oscillation cycles (cf. Figure 3).

- The main characteristics of the erosive damage at the horn tip sample (cf. Figure 2 A-c) can be qualitatively assessed on all grid resolutions: no erosive damage directly at the edge of the sample, highest erosive damage at a ring near the edge of the sample and a continuous erosive damage (smaller than at the ring) at the circular surface inside this ring.
- The erosion-sensitive areas at the horn tip sample can be predicted on 90° segment geometry as well as on 360° complete geometry (cf. Figure 2 A), whereas at the counter sample the erosion probability is overestimated near the rotational axis on a 90° segment geometry (cf. Figure 2 B).

Conclusion

We compare the numerically observed erosion-sensitive area to images of the surface contour for both samples under the same operation conditions (cf. Figure 2 A/B). We

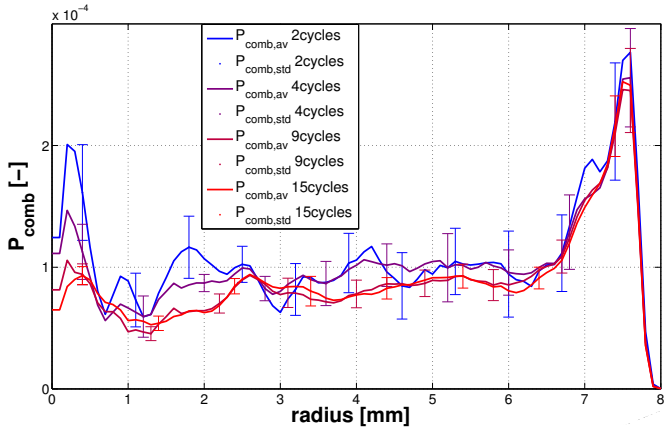

Figure 3: Ambit averaged erosion probability (combined erosion indicator) at the horn tip (cf. Figure 2) for a different number of considered subharmonic oscillation cycles ($P_{comb,av}$). Error bars represent the standard deviation over the ambit ($P_{comb,std}$) as an indicator for the „smoothing“ of the erosion probability profile.

anticipate that the overestimation of the erosion probability at the rotational axis (counter sample; 90° segment geometry) is introduced by the fact, that collapse events near the rotational axis are exponentiated due to pressure wave reflection at the periodic boundaries. This error is - even if it is not quite as pronounced - also present at the horn tip surface (cf. Figure 3). As a requisite consequence, 90° segment geometry will no longer be investigated. In the future, we will repeat the temporal convergence study as well as the grid independency study on a 360° setup in order to ensure that the results presented in this paper are not influenced by the error of the geometry simplification.

References

[1] Dular, M.; Mettin, R.; Žnidarčič, A.; Truong, V. A.: Dynamics of Attached Cavitation at an Ultrasonic Horn Tip. 8th International Symposium on Cavitation (CAV12), Singapore (2012)

[2] Schnerr, G.H.; Sezal, I.H.; Schmidt, S.J.: Numerical investigation of three-dimensional cloud cavitation with special emphasis on collapse induced shock dynamics. Phys. Fluids, Vol. 20 (2008).

[3] Schmidt, S.J.; Sezal, I.H.; Schnerr, G.H.; Thalhamer, M.: Schock Waves as Driving Mechanism for Cavitation Erosion. 8th Int. Symp. Exp. Comp. Aerothermodynamics of Internal Flows (ISAIF), Lyon (2007).

[4] Iben, U.: Modeling of Cavitation. Sys. Anal. Mod. Sim., Vol. 42 (2002)

[5] Mottyll, S.; Müller, S.; Niederhofer, P.; Hussong, J.; Huth, S.; Skoda, R.: Analysis of cavitating flow induced by an ultrasonic horn - Numerical 3D simulation for the analysis of vapour structures and the assessment of erosion-sensitive areas. Exp. Fluid Mech. (EFM), Kutná Hora (2013).